J11.1

# GROUNDWATER–LAND SURFACE–ATMOSPHERE FEEDBACKS: IMPACTS OF GROUNDWATER ON LAND-ATMOSPHERE FLUXES

Ian M. Ferguson* and Reed M. Maxwell
Colorado School of Mines, Golden, Colorado

## 1. INTRODUCTION

Recent studies have demonstrated significant feedbacks between water table dynamics and surface-atmosphere water and energy fluxes (Maxwell et al. 2007, Kollet and Maxwell 2008, Maxwell and Kollet 2008, Ferguson and Maxwell 2010). These studies identify three regimes of the surface water and energy balance with respect to groundwater depth *D*. In regions of shallow groundwater ($D < \sim 10^0$ m), moisture is readily transported from the water table to the land surface; land-atmosphere fluxes over these regions are predominately energy limited and controlled by atmospheric conditions (temperature, wind, humidity, and incoming radiation). In regions of deep groundwater ($D > \sim 10^1$ m), the water table is disconnected from the land surface, and land-atmosphere fluxes are moisture limited and predominately controlled by precipitation. Lastly, in regions of intermediate groundwater depth ($D \sim 10^0$ m), small changes in water table depth cause significant changes in moisture availability at the land surface, and land-atmosphere fluxes are directly tied to water table dynamics.

Spatial variations in water table depth contribute to correlated spatial heterogeneity in soil saturation, sensible and latent heat fluxes, and ground temperature (Kollet and Maxwell 2008), which strongly influence atmospheric boundary layer development (Maxwell et al. 2007). In addition, land surface and hydrologic response to changing climate conditions are also strongly dependent on groundwater (Maxwell and Kollet 2008, Ferguson and Maxwell 2010).

These studies suggest water table dynamics are an important driver of spatial heterogeneity of land surface conditions and land-atmosphere fluxes over some regions. Spatial heterogeneity of land-atmosphere fluxes influence atmospheric boundary layer development, including turbulent mixing and organized convection, and have the potential to significantly feed back on regional climate (Holt et al. 2004, Patton et al. 2005, Maxwell et al. 2007).

Here we use ParFlow, a full-integrated watershed model, to investigate the influence of groundwater on the spatial heterogeneity of land-atmosphere fluxes, focusing on variations in the magnitude of groundwater-land surface feedbacks between seasons and under changing climate conditions. ParFlow is then coupled to the Weather Research and Forecasting Model, a mesoscale atmospheric and regional climate model, to assess the influence of groundwater on simulated land-atmosphere fluxes.

## 2. MODELS AND SIMULATIONS

Four watershed (off-line) simulations and four land-atmosphere (coupled) simulations are analyzed here. All simulations were carried out over the Little Washita River watershed (~700km$^2$) in central Oklahoma, in the Southern Great Plains of North America. The Little Washita watershed and has been the focus of several field campaigns and lies within the US Department of Energy Atmospheric Radiation Measurement Program (ARM) and Oklahoma Mesonet monitoring area, which provide an abundance of high-quality hydrologic and meteorological observations over the area.

### 2.1 *Watershed Simulations*

Watershed simulations were carried out with ParFlow, a variably-saturated groundwater flow model with fully integrated land surface, vegetation, and overland flow processes. ParFlow solves the variably-saturated Richards equation in three dimensions for subsurface flow (Ashby and Falgout 1996, Jones and Woodward 2001). Overland flow and groundwater–surface water interactions are represented through a free-surface overland flow boundary condition, which routes ponded water via the kinematic wave equation and Mannings equation (Kollet and Maxwell 2006). ParFlow incorporates a state-of-the-art land surface model, the Common Land Model (CLM; Dai et al. 2003), to solve the coupled water and energy balance at the land surface (Maxwell and Miller 2005, Kollet and Maxwell 2008). CLM calculates evaporation from the vegetation canopy and the ground surface, transpiration from plants, ground heat flux, freeze-thaw processes, and latent and sensible heat fluxes based on air temperature, wind speed, specific humidity, and solar radiation, soil moisture, and soil and vegetation properties.

ParFlow was configured over a 32km by 45km domain encompassing the Little Washita watershed. The domain was discretized with a lateral resolution ($\Delta x = \Delta y$) of 1km and a vertical resolution ($\Delta z$) of 0.5m. The lowest model layer has uniform elevation of 256m above mean sea level, and subsurface depths range from 63m to 191m based on topography. Spatially distributed vegetation cover and soil parameters in the top model layer (at the land surface) were defined based on USGS observational datasets. Given sparse subsurface observations, uniform soil parameters were applied over the deeper subsurface based on analysis of public records from some 200 boreholes in the region; for complete information, see Kollet and Maxwell (2008).

Four one-year simulations were carried out, including one control and three perturbation scenarios. The control simulation (CNTRL) was based on water-year 1999 (September 1, 1998 to August 31, 1999) and was forced with spatially uniform atmospheric conditions derived from the North American Regional Reanalysis (NARR; Mesinger et al. 2006). Time series of daily precipitation and temperature from CNTRL are shown in Figure 1.

Detailed evaluation of CNTRL against measured soil moisture, latent heat flux, and streamflow was carried out by Kollet and Maxwell (2008). CNTRL was shown to capture the major wetting and drying cycles of observed soil moisture and the seasonal and diurnal cycle of observed latent heat flux over water year 1999 (Kollet and Maxwell 2008). Stream discharge in CNTRL is characterized by flashy response to precipitation events followed by quick recession to baseflow, similar to observed discharge at USGS gauging station 7327550, located near the watershed outlet. Notable differences between simulated and observed streamflow include slight overestimation of storm peaks during winter and spring, and intermittency of simulated streamflow during the summer low-flow season (not shown; refer to Kollet and Maxwell 2008 for details). While observed discharge does not fall to zero, observed flows are below 0.2 $m^3s^{-1}$ during the low-flow season; intermittency in simulated streamflow results from the 1km lateral resolution used here, which inhibits resolution of summer low flows.

Three perturbation scenarios were carried out to evaluate sensitivity of the land surface water and energy balance over the Little Washita watershed to changes in temperature and precipitation: (1) uniform 2.5 ℃ increase in air temperature, all other forcings unchanged (HOT); (2) uniform 2.5 ℃ increase in air temperature, 20% increase in precipitation (HOT-WET); and (3) 2.5 ℃ increase in air temperature, 20% decrease in precipitation (HOT-DRY). It should be noted that temperature perturbations approximate the median projected warming by mid-21$^{st}$ century from the IPCC Fourth Assessment Report, while precipitation perturbations capture the broad range and large uncertainty of projected precipitation changes (Christensen et al. 2007).

All four simulations were carried out to equilibrium by repeatedly driving the model over water-year 1999 with observed or perturbed forcings, respectively, until the water and energy balance over the year reached equilibrium, defined here as a change in water and energy balance over the domain of less than $10^{-6}$ percent over the year.

### 2.2 *Land-Atmosphere Simulations*

Coupled land-atmosphere simulations were carried out with PF.WRF, a new, state-of-the-art, fully-coupled climate and hydrology model (Maxwell et al. 2010). PF.WRF was developed by coupling ParFlow with the Weather Research and Forecasting Model (WRF), a non-hydrostatic, mesoscale atmosphere and regional climate model (Skamarock et al. 2007). WRF solves the compressible, non-hydrostatic Navier-Stokes equations using a robust flux-conservative, time-split integration scheme, and features a positive-definite advection scheme and a number of convection, microphysics, and radiative transfer options.

Coupled simulations were configured for the same domain and resolution as off-line simulations described above. Four simulations were carried out with different land surface and microphysics components. The first two simulations were carried out with the standard WRF model, without coupling to ParFlow; one simulation was carried out with the Morrison microphysics package (WRF-Morrison) and one with the Kessler microphysics (WRF-Kessler). Two simulations were then carried out with the fully couple model PF.WRF, again one with the Morrison microphysics (PF.WRF-Morrison) and one with the Kessler microphysics (PF.WRF-Kessler).

The land surface component of each simulation was initialized by off-line spin-up forced with observed meteorological forcings derived from NARR. WRF-Morrison and WRF-Kessler simulations were initialized from an off-line spin-up of the CLM land surface model, without lateral groundwater flow or integrated overland flow. PF.WRF-Morrison and PF.WRF-Kessler were initialized from off-line spin-up of ParFlow.

Simulations were run for 36 hours beginning at 07:00 CST on July 9, 1999. To isolate the effects of land-atmosphere forcing, all simulations were initialized with zero winds and use free-slip rigid wall lateral boundary conditions. Initial temperature and humidity were specified from a sounding profile measured in nearby Norman, OK, at 07:00 on July 9, 1999. Boundary layer development is thus driven by the diurnal variations incoming solar radiation and consequent land-surface fluxes, leading to both convective and stable conditions during the simulation period.

## 3. RESULTS

### 3.1 *Groundwater-Land Surface Feedbacks*

Interdependence between groundwater depth and the surface energy balance is illustrated in Figure 2, which shows monthly mean latent heat flux *LE* from the land surface as a function of water table depth. Each panel in Figure 2 corresponds to different month; each point in a given panel corresponds to an individual model grid cell, and each color represents a different scenario. For clarity, results are shown only for open shrublands, which encompass much of the upper watershed including hilltops, hillslopes, and upper reaches of the Little Washita river valley.

*LE* exhibits a distinct seasonal cycle in all scenarios. Increasing *LE* from January to June is associated with increasing temperatures (and thus increasing energy availability); decreasing *LE* from July to September are associated with decreasing moisture availability, while decreasing values from October to December are associated with decreasing temperatures.

In the CNTRL (black) scenario, *LE* is strongly dependent on water table depth during the hot, dry summer and autumn months (July-October); during cooler and wetter months, *LE* is largely independent of groundwater depth. The magnitude of groundwater-land surface feedbacks can be quantified as the difference in *LE* between areas of shallow groundwater (taken as $D < 1$m) and areas of deep groundwater (taken as $D > 10$m). Groundwater-land surface feedbacks exceed 75 W/m$^2$ during the warm and dry months of summer and autumn. During these periods, shallow groundwater maintains high moisture availability in areas of shallow groundwater while regions of deep groundwater become strongly moisture limited, resulting in substantial spatial heterogeneity in the land surface water and energy budgets.

In the HOT (green) and HOT-DRY (red) scenarios, *LE* is strongly dependent on groundwater depth throughout more of the year. Under HOT-DRY conditions in particular, groundwater feedbacks result in spatial gradients of 5 W/m$^2$ or more during all months. By contrast, in the HOT-WET scenario (blue), groundwater feedbacks on *LE* are weaker throughout all months compared to CNTRL.

Dependence between *LE* and water table depth clearly varies between seasons and scenarios, with increased dependence during warmer and drier seasons and scenarios and decreased dependence during colder and wetter seasons and scenarios (see Figure 1). Similar dependence is evident for sensible heat flux, ground temperature, potential recharge (precipitation-evaporation), and soil saturation (not shown). It should be noted that the magnitude and depth of groundwater-land surface feedbacks depend on soil and vegetation types, as well as climate factors (Kollet and Maxwell 2008, Ferguson and Maxwell 2010).

### 3.2 Groundwater *Feedback on Coupled Land-Atmosphere Variability*

Soil moisture and *LE* fields from each of the four land-atmosphere simulations analyzed here are shown in Figures 3 and 4, respectively, at t=27 hours from the simulation start time. In WRF simulations (uncoupled to ParFlow), saturation and *LE* exhibit weak spatial heterogeneity, and heterogeneity is not correlated with topography, vegetation cover, or soil type. In addition, saturation fields differ markedly between WRF-Kessler and WRF-Morrison at time t=27h, despite identical initialization at t=0h.

By contrast, fully coupled simulations with PF.WRF exhibit significant, correlated spatial heterogeneity in saturation and *LE*. High saturation and *LE* occur along the river valleys, where topographically-drive subsurface flow results in groundwater convergence and shallow water table depth. By contrast, low saturation and *LE* occur in hilltop areas, where topographic gradients result in a deep water table. As discussed above, the surface energy balance over areas of deep groundwater is predominately moisture limited and controlled by precipitation; high temperatures and low precipitation during July (Figure 1) result in dry soils over these areas, which in turn limits *LE* (Figures 3-4). Saturation and *LE* in PF.WRF simulations also exhibit spatial heterogeneity associated with soil type and land cover, which are not evident in the WRF-only simulations. Lastly, it is also important to note that in contrast to WRF-only simulations, saturation and *LE* in PF.WRF simulations are weakly dependent on the choice of microphysics package. Spatial heterogeneity in soil saturation, and subsequent impacts on *LE*, significantly alter boundary layer development, including turbulent mixing, convection, and precipitation processes (not shown; see Maxwell et al. 2010).

## 4. CONCLUSIONS

Results presented here demonstrate the strong feedbacks between water table dynamics, the land surface water and energy balance, and the atmospheric boundary layer. Key conclusions are as follows:

(1) Under warm and dry climate conditions, the land surface water and energy balance is predominately moisture-limited and is strongly dependent on groundwater–land surface feedbacks; under cooler and wetter conditions, the water and energy balance is predominately energy limited and independent of groundwater.

(2) Climate change resulting in warmer or drier climate conditions will result in stronger groundwater-land surface feedbacks throughout much of the year; however, climate change resulting in wetter conditions may reduce groundwater-land surface feedbacks, even under warmer conditions.

(3) Groundwater-land surface feedbacks result in significant spatial heterogeneity in land surface conditions and land-atmosphere exchange, and result in decreased sensitivity of simulated land-atmosphere interactions to choice of atmospheric micorphysics parameterizations.

Further analysis is needed to quantify the influence of spatial heterogeneity in land-atmosphere fluxes on meso- and regional-scale weather and climate processes, including heat and moisture transport, convection, and precipitation, under realistic synoptic conditions. In addition, further analysis is needed to evaluate the potential influence of water management practices such as groundwater pumping and irrigation on the coupled land-atmosphere system.

## 5. REFERENCES


Ashby SF and RD Falgout (1996). A Parallel Multigrid Preconditioned Conjugate Gradient Algorithm for Groundwater Flow Simulations. *Nuclear Science and Engineering* 124(1): 145-159.

Christensen JH, B Hewitson, A Busuioc, A Chen, X Gao, I Held, R Jones, RK Kolli, WT Kwon, R Laprise, V Magaña Rueda, L Mearns, CG Menéndez, J Räisänen, A Sarr, and P Whetton (2007). Regional Climate Projections. *Climate Change 2007: The Physical Science Basis. Contribution of Working Group I to the Fourth Assessment Report of the Intergovernmental Panel on Climate Change* [Solomon S, D Qin, M Manning, Z Chen, M Marquis, KB Averyt, M Tignor, HL Miller (eds.)]. Cambridge University Press, Cambridge, UK.

Dai YZ, XB Zeng, RE Dickinson, I Baker, GB Bonan, MG Bosilovich, AS Denning, PA Dirmeyer, PR Houser, GY Niu, KW Oleson, CA Schlosser, ZL Yang (2003). The Common Land Model. *Bulletin of the American Meteorological Society* 84(8): 1013-1023.

Ferguson IM and RM Maxwell (2010). The Role of Groundwater in Watershed Response and Land Surface Feedbacks Under Climate Change. *Water Resources Research*, in review.

Holt TR, D Niyogi, F Chen, K Manning, MA LeMone, and A Qureshi (2006). Effect of Land-Atmosphere Interactions on the IHOP 24-25 May 2002 Convection Case. *Monthly Weather Review* 143(1): 113-133.

Jones JE and CS Woodward (2001). Newton-Krylov-Multigrid Solvers for Large-Scale, Highly-Heterogeneous, Variably Saturated Flow Problems. *Advances in Water Resources* 24(7): 763-774.

Kollet SJ and RM Maxwell (2006). Integrated Surface-Groundwater Flow Modeling: A Free-Surface Overland Flow Boundary Condition in a Parallel Groundwater Flow Model. *Advances in Water Resources* 29(7): 945-958.

Kollet SJ and RM Maxwell (2008). Capturing the Influence of Groundwater Dynamics on Land Surface Processes Using an Integrated, Distributed Watershed Model. *Water Resources Research* 44(2): W02402.

Maxwell RM and NL Miller (2005). Development of a Coupled Land Surface and Groundwater Model. *Journal of Hydrometeorology* 6(3): 233-247.

Maxwell RM, FK Chow, and SJ Kollet (2007). The Groundwater-Land-Surface-Atmosphere Connection: Soil Moisture Effects on the Atmospheric Boundary Layer in Fully-Coupled Simulations. *Advances in Water Resources* 30(12): 2447-2466.

Maxwell RM and SJ Kollet (2008). Interdependence of Groundwater Dynamics and Land-Energy Feedbacks Under Climate Change. *Nature Geoscience* 1(10): 665-669.

Maxwell RM, JK Lundquist, J Mirocha, SG Smith, CS Woodward, AFB Tompson (2010). Development of a Coupled Groundwater-Atmospheric Model. *Monthly Weather Review*, in review.

Mesinger F, G DiMego, E Kalnay, K Mitchell, PC Shafran, W Ebisuzaki, D Jovic, J Woollen, E Rogers, EH Berbery, MB Ek, Y Fan, R Gumbine, W Higgiins, H Li, Y Lin, G Manikin, D Parrish, and W Shi (2006). North American Regional Reanalysis. *Bulletin of the American Meteorology Society* 87(3): 343-360.

Patton EG, PP Sullivan, and CH Moeng (2005). The Influence of Idealized Heterogeneity on Wet and Dry Planetary Boundary Layers Coupled to the Land Surface. *Journal of the Atmospheric Sciences* 62(7): 2078-2097.

Skamarock WC and JB Klemp (2007). A Time-Split Nonhydrostatic Atmospheric Model for Weather Research and Forecasting Applications. *Journal of Computational Physics* 227(7): 3465-3485.

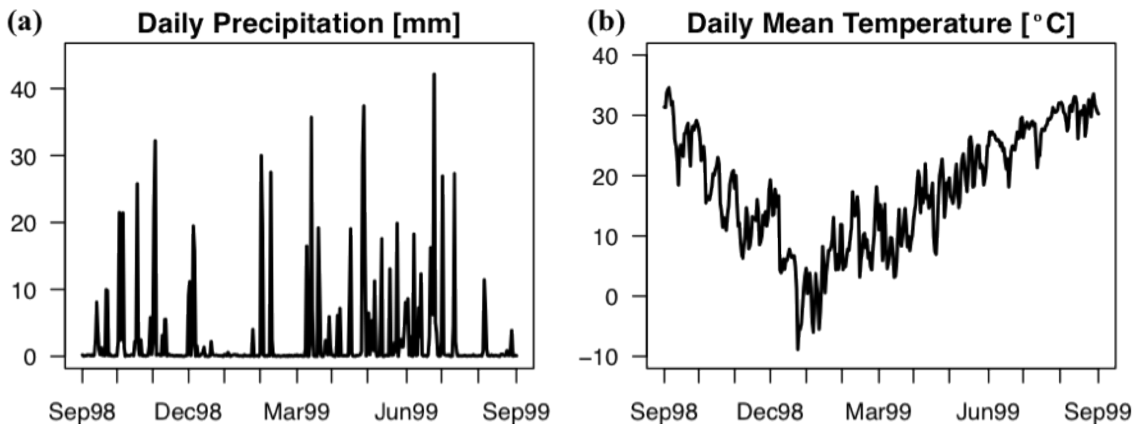


**Figure 1**: Time series of observed daily (a) precipitation and (b) air temperature from water-year 1999 (taken as September 1, 1998, to August 31, 1999) used to force CNTRL simulation.

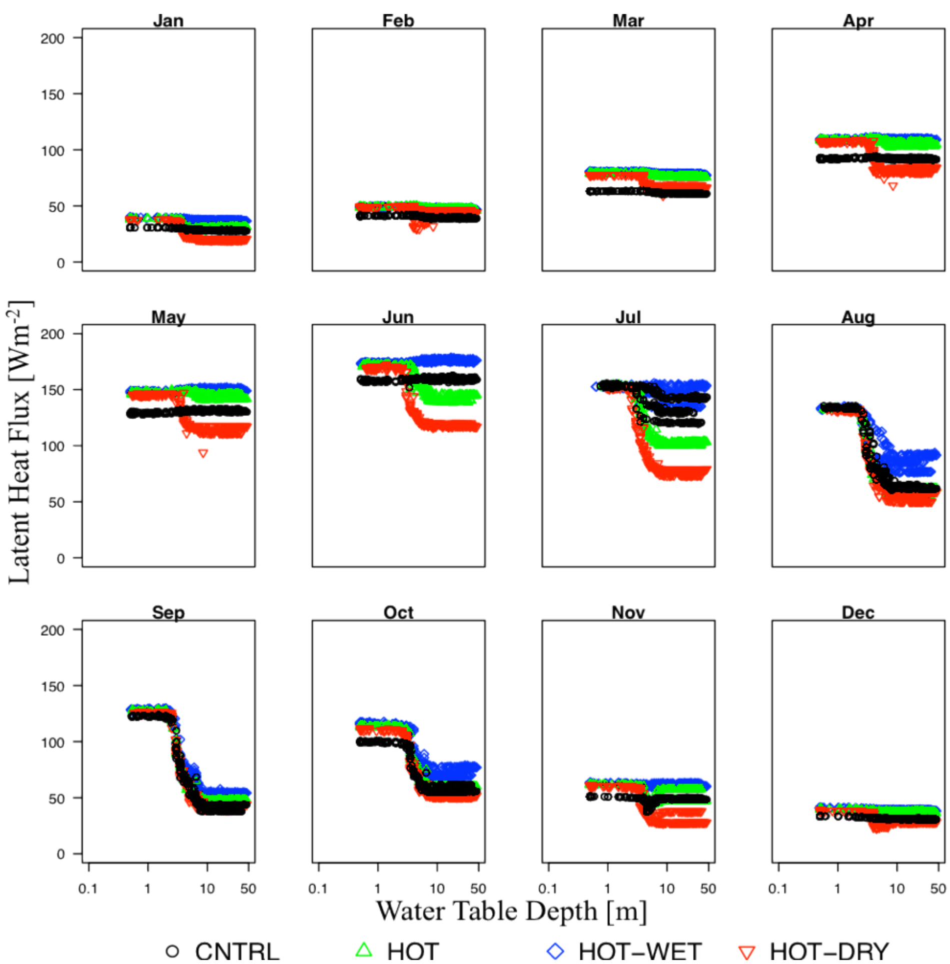


**Figure 2**: Semilog scatterplots of monthly mean latent heat flux [$Wm^{-2}$] as a function of monthly mean water table depth [m] for all four scenarios (black=CNTRL, green=HOT, red=HOT-DRY, blue=HOT-WET).

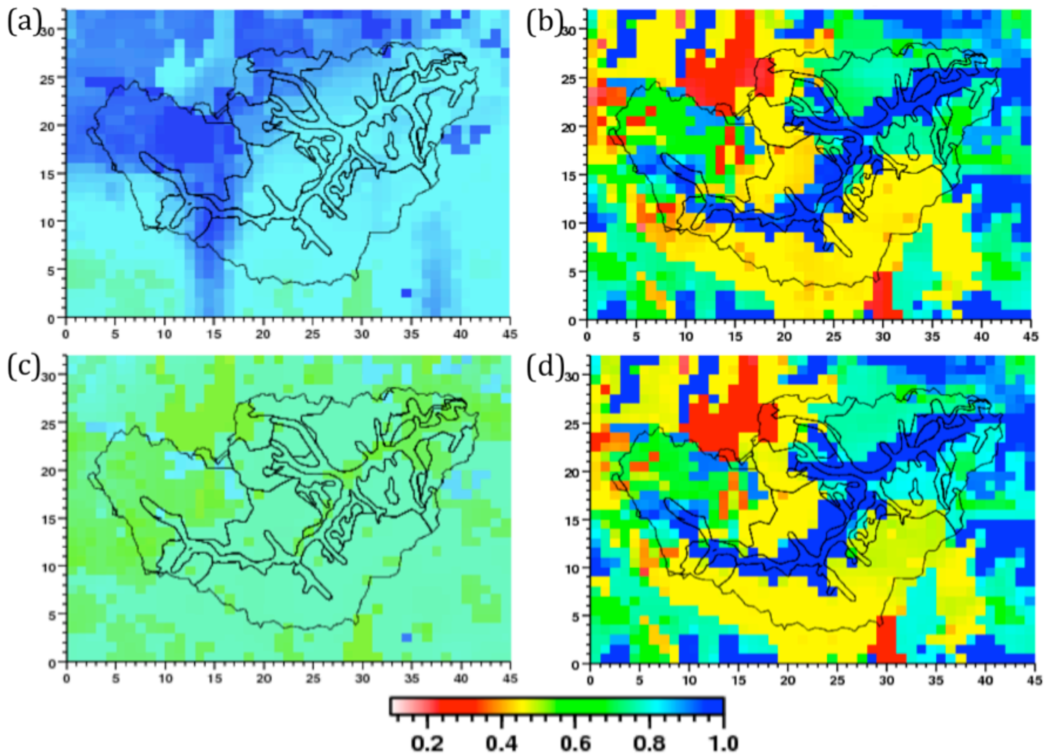


**Figure 3**: Soil saturation [-] at t=27h from simulations (a) WRF-Kessler, (b) PF.WRF-Kessler, (c) WRF-Morrison, and (d) PF.WRF-Morrison.

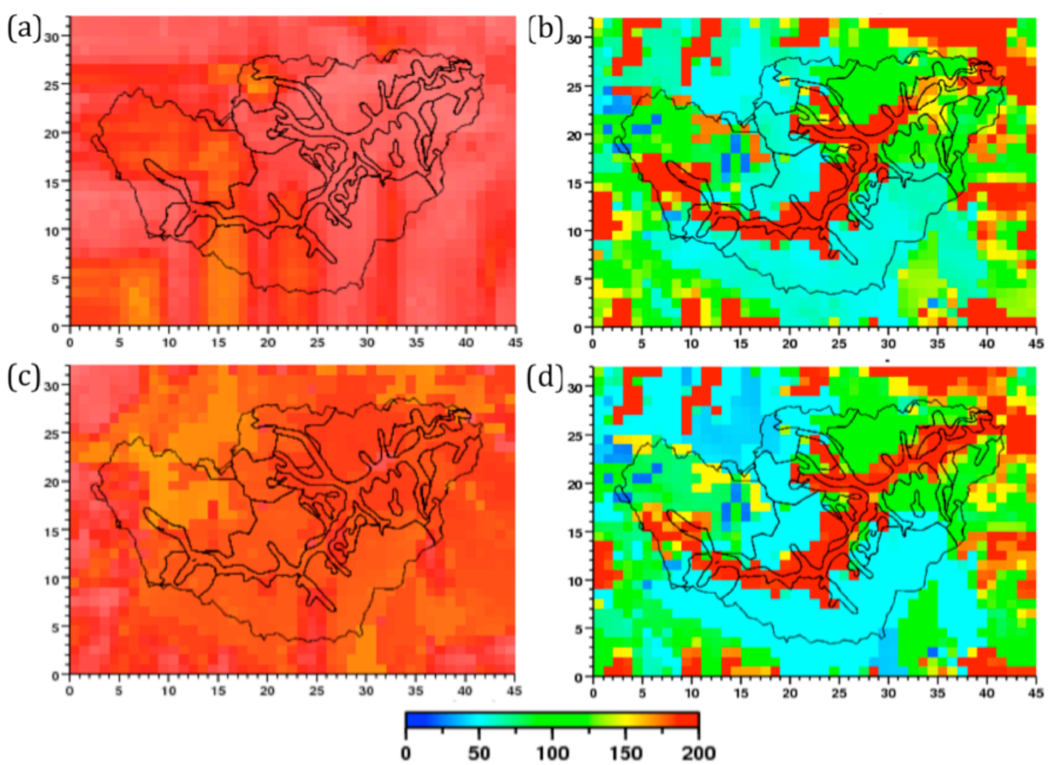


**Figure 4**: Latent heat flux [W/m$^2$] at t=27h from simulations (a) WRF-Kessler, (b) PF.WRF-Kessler, (c) WRF-Morrison, and (d) PF.WRF-Morrison.